



# Thermal behavior of Cu-Mg-Al-Ba/Sr bifunctional composites during chemical looping combustion and HCl adsorption of MSW syngas

Guicai Liu<sup>a,\*</sup>, Xinyi Wu<sup>a</sup>, Ya Zhao<sup>a</sup>, Andrei Veksha<sup>a</sup>, Apostolos Giannis<sup>b</sup>, Teik Thye Lim<sup>a,c</sup>, Grzegorz Lisak<sup>a,c,\*</sup>

<sup>a</sup> Residues and Resource Reclamation Centre, Nanyang Environment and Water Research Institute, Nanyang Technological University, Singapore 637141, Singapore

<sup>b</sup> School of Chemical and Environmental Engineering, Technical University of Crete (TUC), University Campus, 73100 Chania, Greece

<sup>c</sup> School of Civil and Environmental Engineering, Nanyang Technological University, Singapore 639798, Singapore

## ARTICLE INFO

### Keywords:

Waste-to-Energy  
Chemical looping combustion  
Oxygen carrier  
HCl removal  
Sorbent regeneration

## ABSTRACT

Mg-Al-supported composites of CuO Oxygen carrier (OC) and Ba/Sr sorbent synthesized by mechanical mixing were used for three-stage process of MSW syngas chemical looping Combustion and HCl adsorption (CLCA). The syngas combustion and HCl adsorption efficiencies as well as thermal behavior of the composites were investigated. It was found that the composites exhibited great reactivity and stability during cyclic CLCA process. The Ba/Sr sorbent slightly influenced the redox ability of OC owing to the presence of  $\text{Cu}_2\text{MgO}_3$ , but exhibited no impact on the MSW syngas combustion, achieving nearly full combustion during 20 cycles. Regarding to the conditions for sorbent regeneration, higher  $\text{H}_2\text{O}$  content and temperature facilitated sorbent regeneration, allowing better HCl adsorption at fuel reaction stage. The sorbent regeneration conditions were optimized at 60 vol%  $\text{H}_2\text{O}$  and 900 °C. Ba-loading composite exhibited better HCl adsorption performance than the Sr-loading during 20 CLCA cycles maintaining 25–35 ppmv HCl in flue gas because of its better regeneration efficiency (~95%). The CuO/Cu migration to the surface enhanced the stability on mechanical strength, elemental composition and redox ability without appearing significant agglomeration during 20 cycles, maintaining the stability in the reactivity with MSW syngas for long-term operation.

## 1. Introduction

Global efforts in achieving carbon neutral economies, addressing global warming and climate change are constantly explored [1,2]. For example, waste-to-energy (WtE) technologies not only can reduce and utilize the waste for sustainable development, but also accelerate the carbon neutral target due to the biogenic fraction and prevention of methane emissions from landfills [3]. Gasification is one of WtE technologies that offers possibility to efficiently utilize the Municipal solid waste (MSW) to produce syngas for energy generation. However, in this process there are some challenges limiting the efficient utilization of syngas, e.g. the presence of chlorine compounds can cause a high-temperature corrosion of heat recovery system in the WtE plant [4,5] or the possibility of formation of cancerogenic polychlorinated dibenzo-p-dioxins and polychlorinated dibenzo-p-furans (PCDD/Fs) [6].

Nowadays, over 2,430 WtE plants are operating globally, and >2,700 plants with an MSW capacity of 530 million tonnes are forecast to be

operational by 2027 [7]. Due to the rapid development of WtE, Chemical looping combustion (CLC) technology owing to its carbon capture abilities can significantly contribute to the reduction in the greenhouse emissions making the process more environmentally friendly [8,9]. CLC technology uses lattice oxygen from the Oxygen carrier (OC), instead of molecular oxygen, to combust fuel into  $\text{CO}_2$  and  $\text{H}_2\text{O}$ . The lattice oxygen in the OCs is then regenerated by air in two separated interconnected reactors. Without the dilution by nitrogen from air, the  $\text{CO}_2$  in the flue gas in the CLC process can be concentrated, facilitating efficient  $\text{CO}_2$  capture. When applied for the combustion of MSW and MSW-derived fuels, CLC can limit the formation of PCDD/Fs and  $\text{NO}_x$  by-products due to the indirect contact between fuel and gaseous oxygen [10–12]. In the stand-alone CLC system, however, the impurity in form of HCl vapor is still present in the flue gas, resulting in unfavorable corrosion of heat recovery system in WtE plant

To remove HCl from syngas at high temperature, efforts have been made to integrate sorbents into oxygen carriers by forming composite

\* Corresponding authors at: Residues and Resource Reclamation Centre, Nanyang Environment and Water Research Institute, Nanyang Technological University, Singapore 637141, Singapore (G. Lisak).

E-mail addresses: [garner.liu@ntu.edu.sg](mailto:garner.liu@ntu.edu.sg) (G. Liu), [g.lisak@ntu.edu.sg](mailto:g.lisak@ntu.edu.sg) (G. Lisak).

<https://doi.org/10.1016/j.cej.2021.132871>

Received 23 August 2021; Received in revised form 3 October 2021; Accepted 4 October 2021

Available online 9 October 2021

1385-8947/© 2021 The Author(s).

Published by Elsevier B.V. This is an open access article under the CC BY-NC-ND license

(<http://creativecommons.org/licenses/by-nc-nd/4.0/>).

materials. Previously, alkali metal oxides including  $K_2O$  and  $Na_2O$  were loaded on  $Fe_2O_3$ -based OCs for simultaneous syngas combustion and HCl removal, exhibiting 30–80% dechlorination efficiency during 60 cycles [13]. Calcium-containing OC  $CaSO_4/Fe_2O_3$  was also adopted for polyvinylchloride CLC and exhibited HCl adsorption capacity [14]. It was found however that the addition of  $Na_2O$ ,  $K_2O$  and  $CaO$  may cause sintering and agglomeration of OC particles due to the low melting points of generated chlorides ( $NaCl$ : 801 °C,  $KCl$ : 770 °C,  $CaCl_2$ : 772 °C). Furthermore, at high syngas temperatures, the formed  $NaCl$  and  $KCl$  are volatile and could be vaporized causing corrosion [15]. Considering these findings, our previous studies provided an improved composite material consisting of iron ore particles loaded with barium-based sorbent. The composite was able to effectively remove HCl from 500 ppmv to approx. 30 ppmv at high moisture content and high temperature condition during CLCs [16,17]. Due to the saturation by HCl, the activity of sorbents typically decreases and a regeneration stage is required to prolong their lifespan. In a so-called three-stage Chemical looping combustion-adsorption (CLCA) process using the Oxygen carrier sorbent (OCS) composite, besides the fuel reactor for syngas combustion and dechlorination and the air reactor for regenerating lattice oxygen, an additional reactor was added after the air reactor to regenerate the saturated HCl sorbent using water vapor. By testing syngas containing 500 ppmv HCl, compared to the gradual increase of emitted HCl concentration with CLC cycles, the HCl emission was maintained 20–30 ppmv during 5 CLCA cycles using Ba and Sr loaded composites [18].

While previous studies have shown that iron ore based OCs have high activity towards the combustion of CO and  $H_2$  [19,20], which are the main syngas components, their activity towards combustion of methane is generally low [21,22]. Depending on the gasification process, syngas contains 1–4 vol% methane, which accounts for 15–30 % of syngas lower heating value [23,24]. For complete combustion of MSW syngas, Cu-based OCs were adopted due to their high activity towards methane combustion [25,26] with extensive experience even in pilot-scale operation [9]. Due to the low melting point of metallic Cu (1083 °C), various supports, such as  $Al_2O_3$ , MgO,  $SiO_2$ ,  $MgAl_2O_4$ ,  $ZrO_2$  [27–30], are necessary to support the Cu-based OCs. Amongst them,  $MgAl_2O_4$  is promising due to its high mechanical strength and no interaction with CuO avoiding the decline of redox activity [31–33]. While doping with HCl sorbent to form bifunctional composite materials, the interaction between CuO and the sorbents might impact its redox activity. The formation of  $CaCu_2O_3$  and  $Ca_2CuO_3$  was reported to hinder the oxygen release kinetics in the limestone-supported Cu-based OCs [34]. The addition of  $Na_2O$  and  $K_2O$  decreased oxygen uncoupling rate of CuO due to their lower melting points leading to sintering [35]. Similarly, the addition of Ba or Sr additive as HCl sorbent might influence the redox ability by interacting with CuO or support. However, the study on the interaction between CuO, support and sorbents, as well as how the interaction would influence the redox ability of CuO during redox cycles is absent.

In this study, bifunctional composite materials such as Cu-Mg-Al-Ba and Cu-Mg-Al-Sr were developed. Their performances of HCl adsorption, syngas combustion, sorbent regenerability and stability were evaluated in a gas switching fluidized bed reactor. Furthermore, the thermal behavior of composites and the interactions among oxygen carrier, support, and sorbent during CLCA process were systematically investigated.

## 2. Materials and methods

### 2.1. Materials

The OCS composites were prepared with mechanical mixing. CuO (<10  $\mu m$ , Sigma Aldrich), MgO (Sinopharm),  $\gamma-Al_2O_3$  (commercial support, Hangzhou Zhi Hua Jie Technology Co., Ltd.) and  $BaCO_3$  (Sigma Aldrich) or  $SrCO_3$  (Sigma Aldrich) were mixed with deionized water (weight ratio solid : water = 2 : 5), the generated paste was transferred

to a planetary ball mill (Retsch PM100 planetary) with the rotation speed of 350 rpm for 2 h. Subsequently, the precursors were dried at 105 °C for over 6 h, and calcined in a chamber furnace, in which the materials were heating to 1000 °C with the heating rate of 5 °C/min and maintained at 1000 °C for 5 h. Finally, the materials were crushed and sieved to 250–450  $\mu m$  particle size. The mass ratio of CuO:MgO: $Al_2O_3$ :sorbent was 30:16.9:41.1:10 and MgO: $Al_2O_3$  molar ratio was 1:1, where  $BaCO_3$  or  $SrCO_3$  were used as the sorbents. The synthesized composites were labeled as CuMABa and CuMASr, respectively. For comparison, the OC without a sorbent was prepared with the CuO:MgO: $Al_2O_3$  mass ratio of 30:19.7:50.3 and labeled as CuMA.

### 2.2. Reactivity tests

The combustion and HCl adsorption efficiencies of composite materials were evaluated in a gas switching fluidized bed reactor (Fig. 1). The reactor was made by a quartz tube with an inner diameter of 11 mm and a length of 85 cm, and a porous plate was set at the middle to hold the composite samples. In each run, the composite was purged with air during the heating and cooling steps to avoid the oxygen loss. There were three stages for cyclic CLCA process, i.e., (i) fuel reaction (FR) for syngas combustion and HCl adsorption, (ii) air reaction (AR) for regeneration of lattice oxygen in OC, and (iii) sorbent regeneration (SR), simulating reactions occurring in fuel reactor, air reactor and sorbent regenerator, respectively. At the FR stage, the gas mixture containing 42.6 vol%  $N_2$ , 10 vol% CO, 10 vol%  $H_2$ , 10 vol%  $CO_2$ , 2.4 vol%  $CH_4$ , 25 vol%  $H_2O$  and 460 ppmv HCl was used to simulate MSW syngas, which was referred to  $H_2O$ /air gasification of MSW [36]. An impinger bottle filled with deionized water was used to collect HCl in the product gas, and the cold-dry gas was subsequently analyzed in a gas analyzer (SICK, GME 810), in which CO,  $CO_2$  and  $CH_4$  were measured by nondispersive infrared sensor, and  $H_2$  was measured by thermal conductivity sensor corrected for the interference of other gases. The HCl collected in the impinger bottle was analyzed by an ion chromatograph (IC, Dionex ICS-1100). To prevent the HCl condensation before the impinger bottle, the gas lines of the setup were heated to 170 °C. Air was used to regenerate the CuO redox activity at the oxidation stage, while steam was used to regenerate the sorbent at the SR stage. The reaction conditions are provided in Table 1. In the SR stage, air/ $H_2O$  was used to avoid the potential oxygen loss while regenerating the sorbents. Two temperatures (900 °C and 950 °C) and three  $H_2O$  concentrations (125, 250 and 375 sccm, representing 33, 50 and 60 vol%  $H_2O$ ) were applied during SR stage to analyze their effects on sorbent recovery. Additionally, the activity of the composites during CLC cycles (without SR) was tested for comparison. Each run was duplicated, and the results were presented as the average values and error bars.

To evaluate the performance of HCl removal at the FR stage, dechlorination efficiency ( $\eta_{Cl}$ ) was defined and calculated by:

$$\eta_{Cl} = \left(1 - \frac{Cl}{Cl_{blk}}\right) \times 100\% \quad (1)$$

where  $Cl$  and  $Cl_{blk}$  are chlorine amounts collected at the outlet of reactor with and without composite, respectively.

Regeneration efficiency ( $\eta_R$ ) was used to characterize the regenerability of sorbent component in composites, and calculated as:

$$\eta_R = \frac{Cl_{SR}}{Cl_{SR} + Cl_{OCS}} \times 100\% \quad (2)$$

where  $Cl_{SR}$  and  $Cl_{OCS}$  are chlorine amounts desorbed in SR stage and fixed in the OCS composites, respectively.

### 2.3. Characterization technologies

The thermal behavior of composites and the interactions between sorbent and oxygen carrier were investigated by several techniques. The crystalline components were characterized by X-ray diffraction (XRD),

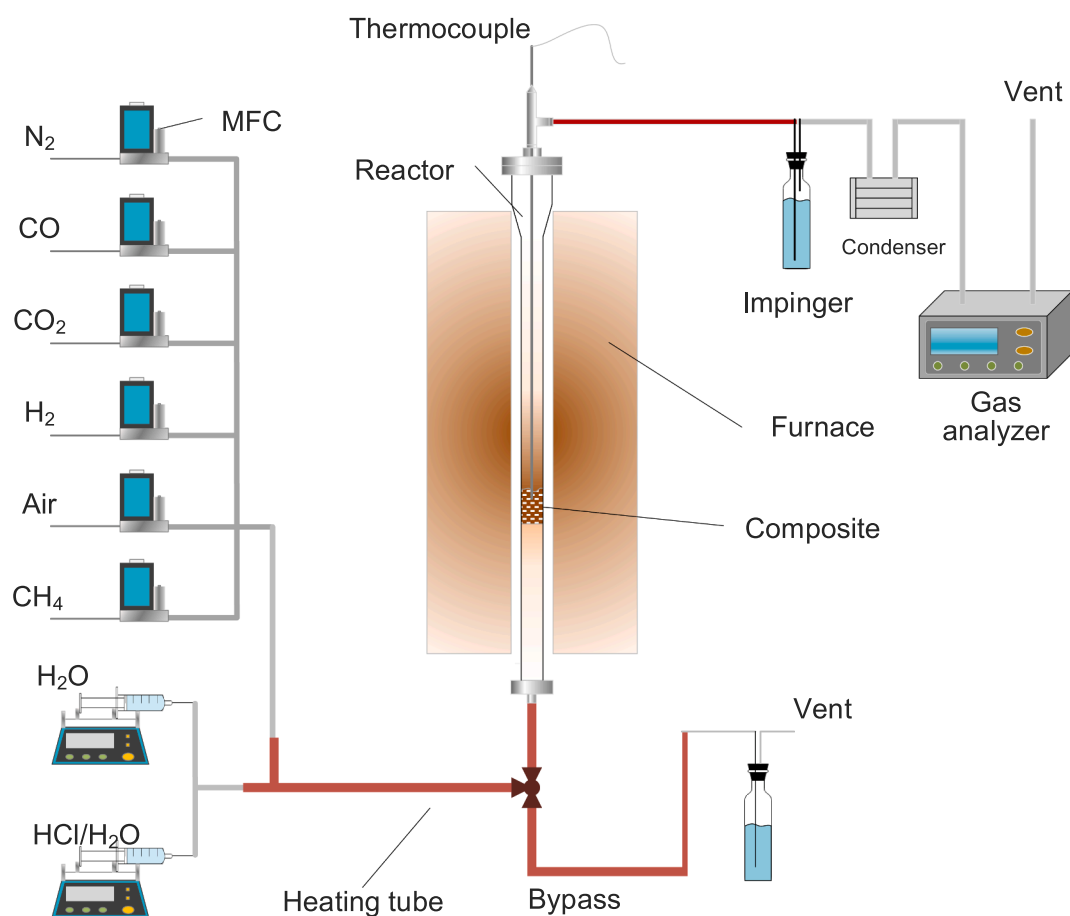


Fig. 1. Gas switching fluidized bed setup for reactivity tests.

**Table 1**  
Reaction conditions for one cycle.

Sequence	Gas	Total gas flow (sccm, wet basis)	Temperature	Duration (min)
Purge 1	N <sub>2</sub>	400	From SR temperature ( $T_{SR}$ ) to 850 °C	5
FR	Simulated syngas	500	850 °C	7
Purge 2	N <sub>2</sub>	400	850 °C	5
AR	Air	400	850 °C to 950 °C (10 °C/min)	10
Purge 3	Air	250	From 950 °C to $T_{SR}$	2
SR	Air, H <sub>2</sub> O	Air: 250; H <sub>2</sub> O: 125/250/375	$T_{SR}$ : 900 °C, 950 °C	21

Bruker D8 Advanced). The morphology, porosity and crushing strength were analyzed with field-emission scanning electron microscopy with energy dispersive spectroscopy (FESEM-EDS, JSM-7200F, JEOL), N<sub>2</sub> adsorption (Micromeritics ASAP-2460) and force gauge (Handpi HP-200, mean value of 20-time tests for each sample), respectively. The metal composition was determined by acid digestion followed by inductively coupled plasma - optical emission spectrometry (ICP-OES, Perkin Elmer Optima 8300). The chlorine content in solid samples was measured after water leaching followed by ion chromatography. The details about acid digestion and water leaching are provided in [Supplementary material](#).

The oxygen capacity and redox ability of each composite were analyzed by a thermogravimetry analyzer (TGA, NETZSCH). Two sets of tests were conducted. In the first set, 40 ± 0.1 mg composite was

subjected to air (250 ml/min), pure N<sub>2</sub> (250 ml/min) and CO/N<sub>2</sub> (10 ml/min CO and 250 ml/min N<sub>2</sub>) in the following order under 850 °C: air (10 min) → N<sub>2</sub> (40 min) → air (5 min) → CO/N<sub>2</sub> (25 min) → air (5 min). The oxygen uncoupling capacity (OUC) and total oxygen capacity (TOC) were defined to characterize the capacity of decomposing to gaseous oxygen and reducing by CO, respectively, and were calculated as:

$$OUC = \frac{m_0 - m_N}{m_0} \quad (3)$$

$$TOC = \frac{m_0 - m_{CO}}{m_0} \quad (4)$$

where  $m_0$  is the initial mass OCS composites, and  $m_N$  and  $m_{CO}$  are the final masses under N<sub>2</sub> and CO/N<sub>2</sub> atmosphere, respectively.

In the second set, a temperature program reduction with CO (CO-TPR) was used to compare the redox ability of each composite. In each run, 20 ± 0.1 mg composite was subjected to a gas mixture of 10 ml/min CO and 250 ml/min N<sub>2</sub>. The temperature was increased from 100 °C to 600 °C with the heating rate of 5 °C/min.

### 3. Results and discussion

#### 3.1. Characterization of fresh composites

The crystalline phase composition of prepared composites is presented in Fig. 2. Without the sorbent loading, the OC CuMA was mainly composed of CuO (#05–0667) and MgAl<sub>2</sub>O<sub>4</sub> (#21–1152), and a small amount of Cu<sub>2</sub>MgO<sub>3</sub> (#41–1365). These results suggest that during calcination MgO reacted with both CuO and Al<sub>2</sub>O<sub>3</sub>. However, there was no evidence that the crystalline phase formation attributed to the reaction between CuO and Al<sub>2</sub>O<sub>3</sub>. Since the formation of Cu-Al mixed

a: CuO (#05-0667) b: MgAl<sub>2</sub>O<sub>4</sub> (#21-1152) c: Cu<sub>2</sub>MgO<sub>3</sub> (#41-1365)  
d: BaAl<sub>2</sub>O<sub>4</sub> (#17-0306) e: SrAl<sub>2</sub>O<sub>4</sub> (#31-1336)

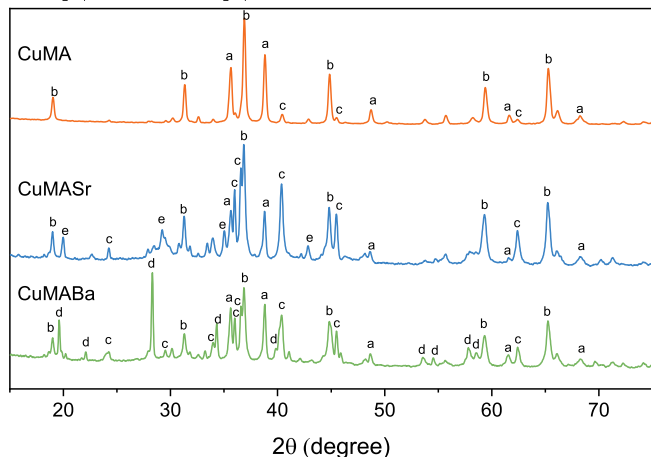


Fig. 2. XRD patterns of fresh OCS composites.

oxide (i.e., spinel CuAl<sub>2</sub>O<sub>4</sub>) would lead to the loss of redox ability [32,37] and oxygen capacity due to the difficult oxidation of the reduced product CuAlO<sub>2</sub> [38], the loss of redox ability in this case was avoided. The formation of Cu<sub>2</sub>MgO<sub>3</sub> could be due to the excess MgO in the precursors. In the CuMABa and CuMASr composites, the crystalline phases of BaAl<sub>2</sub>O<sub>4</sub> (#17-0306) and SrAl<sub>2</sub>O<sub>4</sub> (#31-1336) were identified, respectively, suggesting that BaCO<sub>3</sub> and SrCO<sub>3</sub> interacted with Al<sub>2</sub>O<sub>3</sub> during calcination. The high intensities of diffraction peaks of BaAl<sub>2</sub>O<sub>4</sub> compared to SrAl<sub>2</sub>O<sub>4</sub> were attributed to the low melting point of precursor BaCO<sub>3</sub> (811 °C), which crystal grain size grew rapidly resulting the higher crystallinity of CuAl<sub>2</sub>O<sub>4</sub> during high-temperature calcination. Both composites also contained crystalline CuO phase. Compared to CuMA, the CuMABa and CuMASr composites had increased XRD peak intensities corresponding to Cu<sub>2</sub>MgO<sub>3</sub> and decreased peak intensities for MgAl<sub>2</sub>O<sub>4</sub>. This could be attributed to the dynamic reactions of Al<sub>2</sub>O<sub>3</sub> with Ba and Sr species. As a result, the excess of MgO could interact with CuO forming more Cu<sub>2</sub>MgO<sub>3</sub>.

The CO-TPR profiles of OCS composites conducted by TGA are shown in Fig. 3. It can be seen there were two weight loss peaks in each material. Since CuO reduced from Cu<sup>2+</sup> to Cu<sup>0</sup> by CO at a temperature range of 160–240 °C [39–41] depending on the synthesis process, the first reduction peak could be assigned to the reduction of CuO. The second reduction peak could be attributed to the reduction of Cu<sub>2</sub>MgO<sub>3</sub>

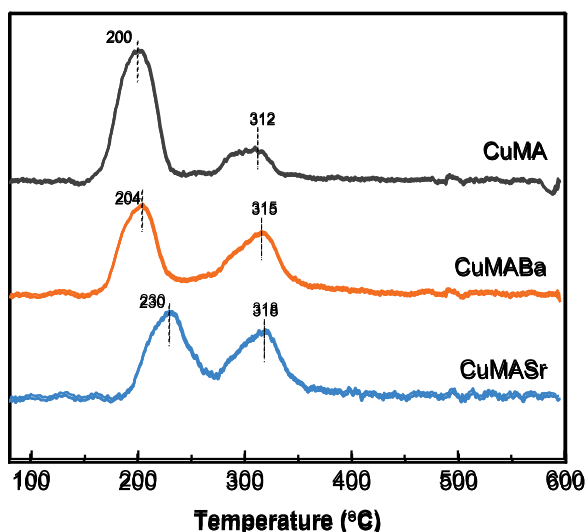


Fig. 3. CO-TPR profiles of the fresh composites.

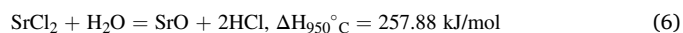
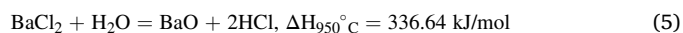
due to its lower activity [42,43] and lower content in CuMA. Since there was higher Cu<sub>2</sub>MgO<sub>3</sub> content of CuMABa and CuMASr than that of CuMA as shown in XRD results (in Fig. 2), more lattice oxygen was presented in lower activity (reduced at higher temperature). Considering the reduction temperatures, the introduction of Ba sorbent slightly increased the reduction temperature, while Sr sorbent addition increased the reduction temperature of CuO → Cu from 200 °C to 230 °C. This implies that the introduction of Ba and Sr sorbents slightly weakened the redox ability of CuMA oxygen carrier. One explanation could be that the addition of Ba/Sr species influenced the dispersion of CuO on the support leading to lower redox ability [44], and the Sr had higher mole fraction than Ba in the composites resulting higher negative effects.

### 3.2. HCl adsorption and sorbent regeneration properties

#### 3.2.1. Optimization of sorbent regeneration conditions

The HCl emissions during 5 cycles of CLC process are shown in Fig. 4 (a). In these experiments, there was no SR, only air regeneration was used to restore oxygen content in the composite. HCl concentrations for CuMA were lower than the blank test, suggesting that small quantities of HCl were removed by the material. This could be attributed to the interaction between CuO and HCl according to the thermodynamic calculation at high temperature and humid conditions reported in [45], but there was no evidence presenting the interaction between HCl and MgAl<sub>2</sub>O<sub>4</sub>. The removal efficiencies of CuMABa and CuMASr were much higher, decreasing the HCl content in effluent gas below approx. 40 ppmv during the first 2 cycles. However, at longer number of cycles, the dechlorination efficiency gradually declined while the HCl emission increased. This was attributed to the saturation of Ba and Sr sorbents due to the lack of regeneration step. Fig. 4(b) and Fig. 4(c) demonstrate the HCl emissions in the effluent gas during CLCA process (with SR in each cycle). Fig. 4(d) and Fig. 4(e) show the corresponding desorption amounts of chlorine at the SR stage. Compared to that without SR, the HCl emissions in the effluent gas significantly decreased, especially after 3–4 cycles. Correspondingly, considerable chlorine was released at the SR stage, suggesting that the regenerability of both composites maintained the HCl adsorption activity for syngas. However, the HCl emissions still had a slight increase with the cycle number, thus it is necessary to optimize the SR conditions.

For optimizing the SR conditions, the chlorine desorption amount at SR stage was compared under different regenerating temperatures and moisture contents. As shown in Fig. 4(d) using CuMABa, regardless of whether the sorbent was regenerated with 50 vol% or 60 vol% H<sub>2</sub>O, the desorbed chlorine amount with 950 °C (solid line) was significantly higher than that of 900 °C (dash line). When CuMASr was used as composite (Fig. 4(e)), 950 °C (solid line) also led to higher chlorine desorption than 900 °C (dash line) at each cycle. Therefore, higher temperature facilitated the regeneration of sorbent. Since the regeneration of Ba and Sr-based sorbent (described in eqs. (5) and (6)) was a highly endothermic process ( $\Delta H > 0$ ), higher temperature would shift the equilibrium towards the right side, leading to the better regeneration.



Besides temperature, moisture content was another important parameter affecting the composite regenerability. The data for CuMABa show that more chlorine could be desorbed during SR stage when the H<sub>2</sub>O content in gas increased from 33 to 60 vol%. Similar behavior was also observed for CuMASr.

In the comparison of HCl emissions between different regeneration conditions (in Fig. 4(b) and (c)), the variation trend was opposite to the chlorine desorption at SR stage. It suggested that HCl adsorption activity was influenced by SR condition indirectly. Better SR conditions, i.e.,

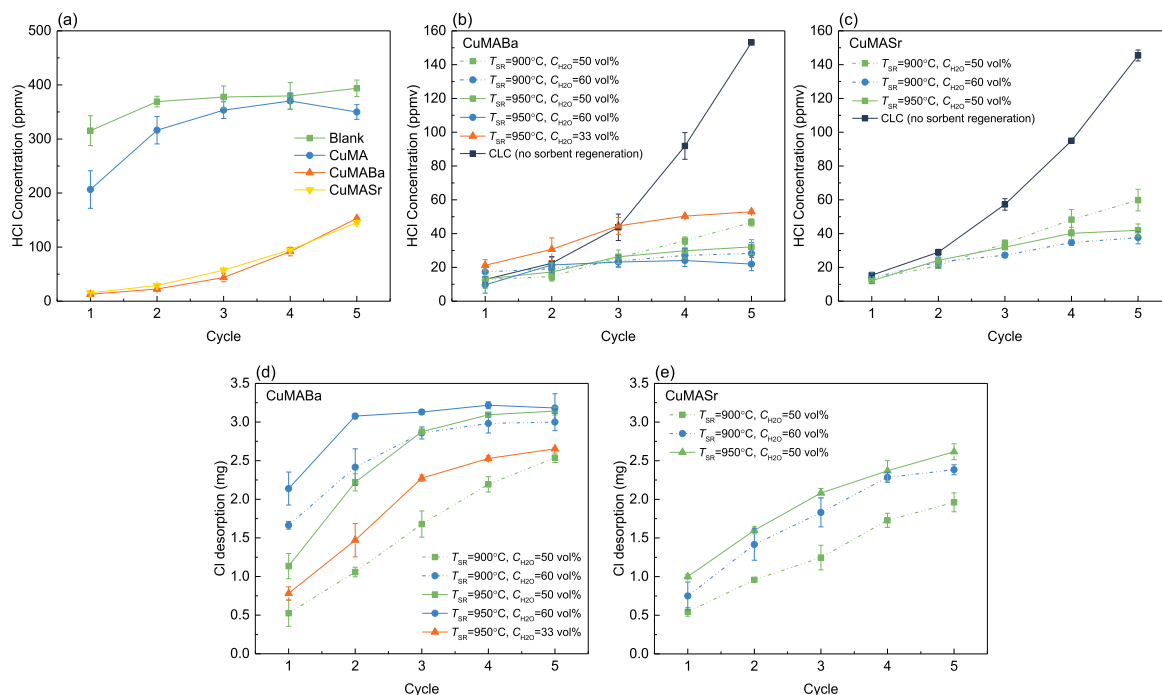


**Fig. 4.** HCl emissions of FR stage during (a) CLC process for composites; (b) CLCA process for CuMABa; (c) CLCA process for CuMASr. Chlorine desorption amounts of SR stage for (d) CuMABa and (e) CuMASr.

higher temperature and  $H_2O$  content, led to higher content of active sorbent in the subsequent cycle, resulting the better HCl adsorption activity.

The obtained results suggest that higher  $H_2O$  content and temperature during SR stage were conducive to the regeneration of sorbent. However, for the industrial application in interconnected fluidized bed, regenerating the sorbent at extremely high temperature might be challenging for auto-thermal operation of the CLCA process. In this study, the HCl emissions were comparable when the composites were regenerated at two SR conditions:  $T_{SR} = 950^\circ C$ ,  $C_{H_2O} = 50 \text{ vol}\%$  and  $T_{SR} = 900^\circ C$ ,  $C_{H_2O} = 60 \text{ vol}\%$  (HCl concentrations could be stabilized at 20–30 ppmv using CuMABa (Fig. 4)). Therefore, the SR temperature could be reduced to  $900^\circ C$  in the design of the interconnected fluidized bed. Figure S1 shows the HCl removal efficiencies during 5 CLC and CLCA cycles. The dechlorination efficiencies were continuously declined during 5 CLC cycles, and decreased to 60–65% at the 5th cycle. With the optimized sorbent regeneration condition, the HCl removal efficiencies did not have a significant decrease during 5 cycles and maintained at the level of  $> 90\%$ .

### 3.2.2. Stability of HCl adsorption and sorbent regeneration processes

To explore the stability of HCl removal in a long-term operation, the evolution of HCl release in the three stages was investigated in 20 cycles (Fig. 5). For both composites, the HCl emissions at FR stage gradually increased at the initial 5–6 cycles, and remained similar in the subsequent cycles. Similarly, the chlorine desorption amounts of SR stage also increased and stabilized after 5–6 cycles. This could be ascribed to the incomplete regeneration of sorbents. At the SR stage of the initial cycles, the desorption of chlorine was inhibited due to the presence of unsaturated sorbents, leading to the decline of dechlorination ability. Simultaneously, with the increase of cycle number, the incomplete regeneration led to the accumulation of  $BaCl_2$  or  $SrCl_2$ , resulting more chlorine to desorb in the SR stage, thus the decline of dechlorination activity would be alleviated. These two effects were balanced after 5–6 cycles, leading to the stable HCl adsorption and chlorine desorption.

It is favorable that all chlorine should be released at SR stage, to prevent corrosion of boiler from the flue gas of fuel reactor and air

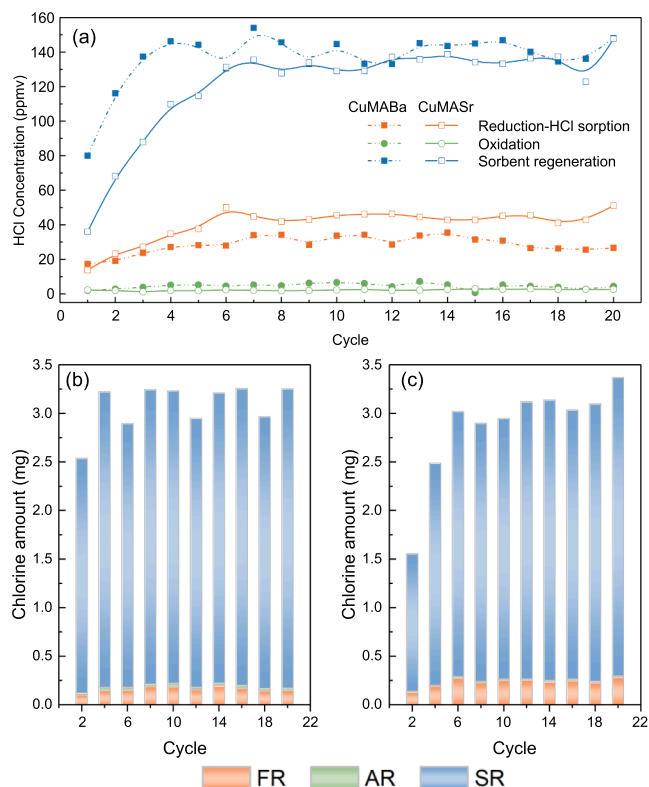


**Fig. 5.** HCl evolution during 20 cycles of CLCA process: (a) HCl release concentration and chlorine release amounts in case of (b) CuMABa and (c) CuMASr (SR:  $T_{SR} = 900^\circ C$ ,  $C_{H_2O} = 60 \text{ vol}\%$ ).

reactor. The comparison of the desorption amounts between each stage during 20 cycles is shown in Fig. 5b and c. After stabilization (5–6 cycles), almost all the chlorine was released at the SR stage, while only small amount of chlorine emitted at FR stage and the chlorine released at

AR stage was negligible, which allowed high-efficient utilization of the gas products.

To validate the inference of incomplete sorbent regeneration and obtain the regeneration efficiencies, the chlorine content of composites before and after reactions are shown in Fig. 6(a). Compared to the fresh composites, considerable chlorine was observed after 5 cycles of CLC process (without SR), verifying the effective HCl adsorption capacity of composites. After 5 cycles of CLCA process (with SR), the chlorine contents were significantly decreased compared with that after 5-cycle CLC, but still significantly higher than the fresh ones. This implies that the sorbents were not completely regenerated during CLCA cycles, explaining the increase of HCl emission at FR stage and chlorine desorption at SR stage. When the CLCA process was extended to 20 cycles, the chlorine contents were continuously increased at a lower rate per cycle. For further explaining the fate of chlorine during CLCA process, the normalized balance of chlorine was calculated and shown in Fig. 6(b). As can be seen, approx. 19% and approx. 34% chlorine were fixed in CuMABa and CuMASr during 1-5th cycle, respectively. During 6-20th cycle (representing almost stabilized stage), the fixed chlorine in CuMABa and CuMASr was decreased to approx. 5% and approx. 7%, respectively. Meanwhile, the chlorine desorption amounts of SR stage were increased from 77% and 60% to 89% and 85% for CuMABa and CuMASr, respectively, suggesting that the composites had higher regeneration efficiency after stabilization. During 6-20th cycles, average regeneration efficiencies of CuMABa and CuMASr were approx. 95% and approx. 92%, respectively.

Comparing CuMABa and CuMASr, the stabilized HCl emission after dechlorination reaction were 25–35 ppmv and 40–50 ppmv, respectively. Simultaneously, the stabilized chlorine desorption amount of SR stage using CuMABa was slightly higher than that of CuMASr, and the chlorine content of regenerated CuMABa was correspondingly lower than regenerated CuMASr. Considering that the HCl capacities of two composites were similar according to CLC tests, it could be concluded that the better HCl adsorption activity of CuMABa was owing to its better sorbent regenerability than CuMASr, instead of its dechlorination capacity. This phenomenon was similar to the one observed in our previous study [18], which showed that Ba-based sorbent exhibited a better regenerability than Sr-based sorbent. One explanation was that the chlorination product  $\text{BaCl}_2$  (969 °C) had a higher melting point than  $\text{SrCl}_2$  (874 °C).  $\text{SrCl}_2$  would be in molten phase during the AR (max. 950 °C) and SR (900 °C) stages, which inhibited the contact with  $\text{H}_2\text{O}$  during regeneration, while  $\text{BaCl}_2$  was still in solid phase leading to better kinetics in regeneration.

### 3.3. Syngas combustion performance

The flue gas composition obtained during FR stage of the first cycle using the three composites is shown in Fig. 7(a-c). With the duration of the experiments, the gas composition changed for the three materials. At

first, all combustible gases, i.e.,  $\text{CO}$ ,  $\text{H}_2$  and  $\text{CH}_4$ , were almost undetectable (7–13 min), except there was  $\text{H}_2$  fluctuation at 7–10 min owing to the error of TCD (thermal conductivity detector) correction by  $\text{CO}_2$ . This corresponds to nearly complete combustion of syngas by the composites. Then, the concentrations of combustible gases gradually increased (13–15 min), which is attributable to the depletion of oxygen in the composites. Based on the similar results, the loading of Ba and Sr sorbent did not have impact on the MSW syngas combustion during the first cycle. Although the formation of  $\text{Cu}_2\text{MgO}_3$  phase in CuMABa and CuMASr was demonstrated to be likely in the lower redox ability [42,43], this was not confirmed by experimental works.

The CuMABa and CuMASr activity in the combustion of syngas during 20 cycles is shown in Fig. 7 (d) and (e). As can be seen, for CuMABa and CuMASr, the  $\text{CO}_2$  concentrations did not show any significant decline during 20 cycles. Simultaneously, the concentrations of combustible gases were also stable.  $\text{CO}$ ,  $\text{H}_2$  and  $\text{CH}_4$  were nearly undetectable before the depletion of lattice oxygen, and their peak values did not have a significant increase during 20 cycles. It can be concluded that both CuMABa and CuMASr have high stability during long term syngas combustion. Since the reactivity of CuMA also exhibited stable during 5 redox cycles (shown in Figure S2), the stability of composites was attributed to the great dispersion of CuO on the support rather than the sorbent addition.

### 3.4. Evolution of composites during CLCA process

The surface morphologies of CuMABa and CuMASr before and after cyclic CLCA process are shown in Fig. 8. The surface of the fresh OCS was composed of granules in hundreds of nanometers, and covered with a layer of loose granules, which might be worn off during fluidization. After 5 cycles, the surface was densified, but nano granules were still remained on the surface, and no significant agglomeration was observed. The EDS mapping shows that Cu element was not distributed evenly as other elements (Mg, Al, Ba and Sr), and the dense surface was mainly composed of Cu compounds. This suggests that Cu/CuO tended to aggregate on the surface during redox cycles with the presence of porous structure, which was similar to the phenomenon in [46,47] exhibiting the migration of active Cu to the surface during redox cycles. At the same time, the formation of dense surface might improve the mechanical strength and attrition resistance during fluidization. After 20 cycles, the surfaces of composites were similar to that after 5 cycles, indicating that the aggregation of Cu/CuO have not deteriorated during long-term operation. Therefore, the good dispersion of Cu compounds on Mg-Al support alleviated the significant agglomeration of composites, stabilizing the reactivity with MSW syngas during long-term operation.

The XRD patterns of used CuMABa and CuMASr show that the crystalline phases changed after 20 cycles (Fig. 9). The  $\text{Cu}_2\text{MgO}_3$  peaks nearly disappeared after 5 and 20 cycles. Similar effects were also found

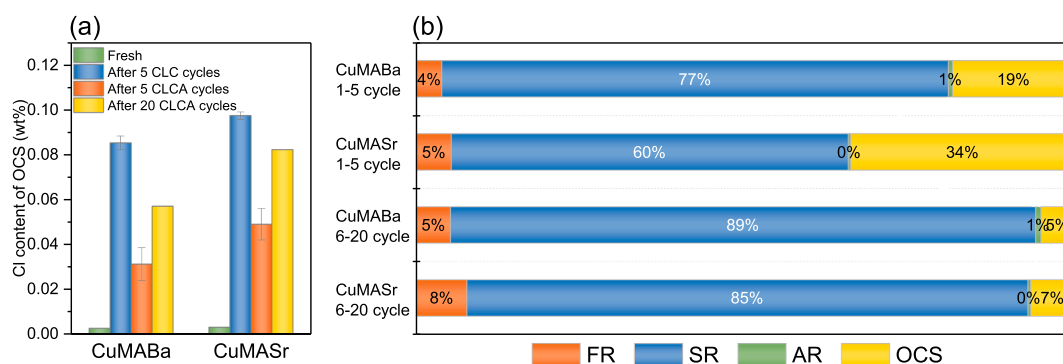


Fig. 6. Chlorine content of fresh and regenerated composites (a) and normalized chlorine balance of composites during CLCA process (SR:  $T_{\text{SR}} = 900$  °C,  $\text{C}_{\text{H}_2\text{O}} = 60$  vol%) (b).

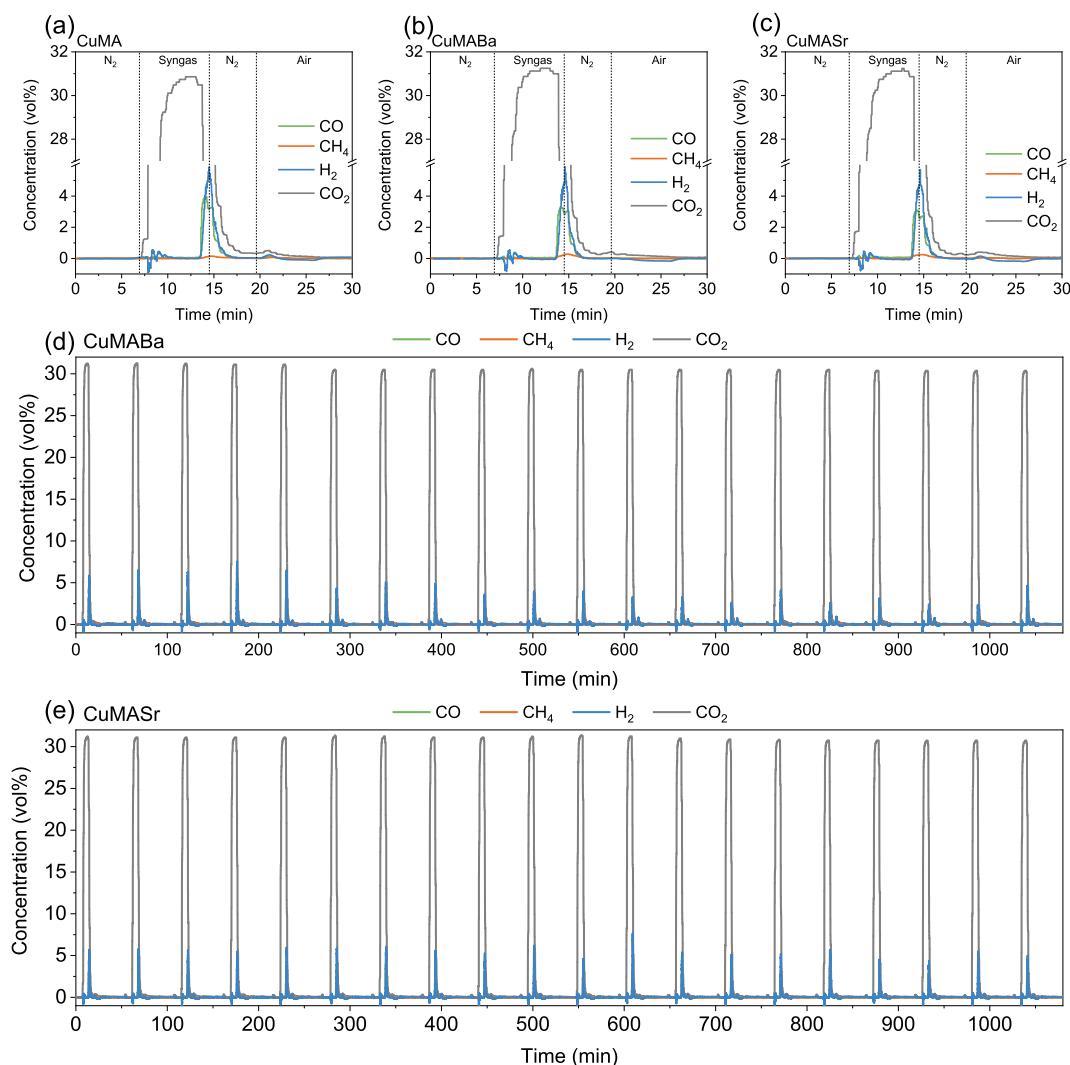


Fig. 7. Concentrations of gas products during CLCA process: (a–c) First cycle; (d) CuMABa in 20 cycles; (e) CuMASr in 20 cycles (SR:  $T_{SR} = 900\text{ }^{\circ}\text{C}$ ,  $C_{H_2O} = 60\text{ vol}\%$ ).

for olivine-supporting CuO in other study [28]. One possible reason was the migration of Cu to surface during redox cycles [46], which led to the uneven distribution of Cu/CuO and limited the dissolution of CuO into the complex oxide  $\text{Cu}_2\text{MgO}_3$ . In addition, the intensity ratio CuO:  $\text{MgAl}_2\text{O}_4$  was getting higher after 5 and 20 cycles. This could be ascribed to the exsolution of CuO during redox cycles and the lower melting point of metal Cu (reduced phase), resulting in the growth of crystalline size. The crystalline chlorides were not detected after 5 and 20 cycles probably due to low contents or amorphous structures.

The composition of materials before and after cyclic CLCA process is shown in Table 2. The actual CuO contents of the fresh OCS were approx. 36%. In the application of Cu-based OCS for chemical looping process, the long-term fluidization and redox cycles might result in the loss of active components due to the attrition [48–50]. Our previous study also showed the decrease of sorbent content (Ba and Sr) after multiple cycles [18]. In this study, after 5 or 20 cycles, the content of each component was hardly changed, suggesting that there was no separation between support, CuO and sorbent during long-term fluidization. On one hand, the strong interaction between support and sorbents improved the mechanical strength by forming  $\text{BaAl}_2\text{O}_4$  and  $\text{SrAl}_2\text{O}_4$ . On the other hand, the dense surface formed by the redox of CuO alleviated the abrasion and improved its mechanical strength. Therefore, the developed composites exhibited great stability in active component content during long-term CLCA operation.

The oxygen capacity and redox ability after multiple cycles were

characterized with TGA (Fig. 10). All composites could be decomposed at N<sub>2</sub> atmosphere, and lost more weight with the reduction of CO. Due to oxygen uncoupling property, CuO was decomposed into  $\text{Cu}_2\text{O}$  and gaseous oxygen. For the fresh composites, the oxygen uncoupling capacities of CuMABa and CuMASr (in Table S1) were 3.04 wt% and 3.02 wt%, respectively, which were higher than that of CuMA (2.76 wt%), thus the introduction of sorbents enhanced the release of gaseous oxygen. Notably, the decomposition rates of regenerated composites were significantly faster than that of fresh ones, although there was no difference between oxygen uncoupling capacities of fresh and regenerated composites. It could be attributed to the migration of Cu/CuO to surface during redox cycles, which facilitated the diffusion of generated gaseous oxygen on the surface, leading to the acceleration of the oxygen uncoupling process. For the reduction under CO/N<sub>2</sub> atmosphere, there was no significant difference among the TG curves of all composites, and the total oxygen capacities were approx. 6 wt%. Hence, the multiple cycles did not influence the redox ability and oxygen capacity of each composite.

The comparison of CO-TPR profile between fresh and regenerated OCSs is shown in Fig. 11. For CuMABa, after 5 or 20 CLCA cycles (with SR), the second reduction peak (320–340 °C) associated with the reduction of  $\text{Cu}_2\text{MgO}_3$  gradually disappeared, which was consistent with the disappearance of  $\text{Cu}_2\text{MgO}_3$  in the XRD patterns (Fig. 9). The reduction peak at approx. 220 °C was corresponding to the reduction of CuO. However, after 5 CLC cycles (without SR), another reduction peak

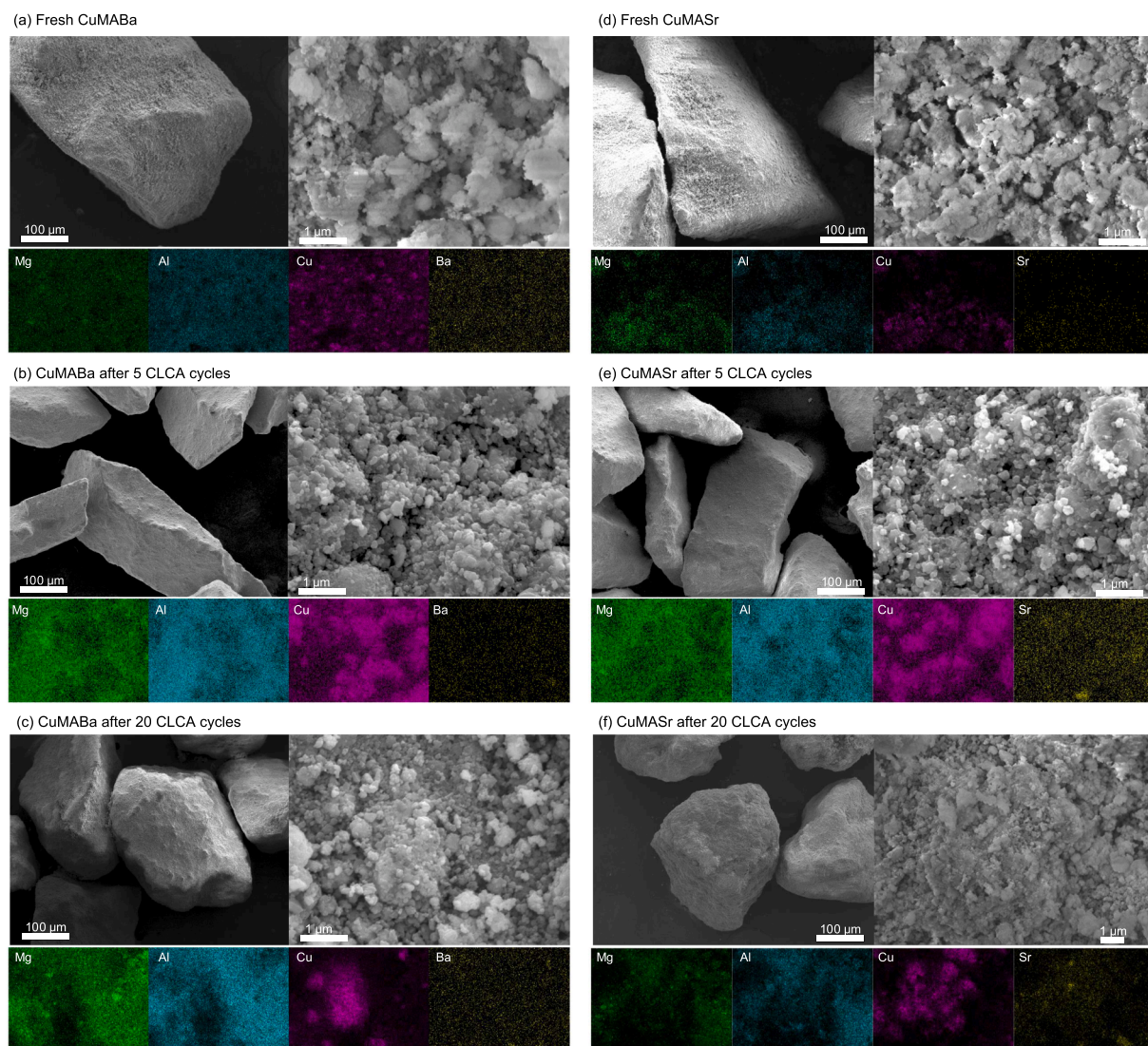


Fig. 8. FESEM images of composites before and after cyclic CLCA reactions (SR:  $T_{SR} = 900\text{ }^{\circ}\text{C}$ ,  $\text{C}_{\text{H}_2\text{O}} = 60\text{ vol}\%$ ).

a: CuO (#05-0667) b:  $\text{MgAl}_2\text{O}_4$  (#21-1152) c:  $\text{Cu}_2\text{MgO}_3$  (#41-1365) d:  $\text{BaAl}_2\text{O}_4$  (#17-0306)  
e:  $\text{SrAl}_2\text{O}_4$  (#31-1336)

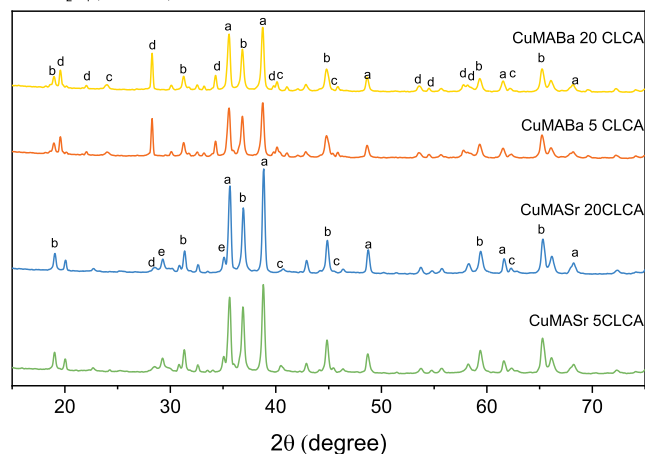


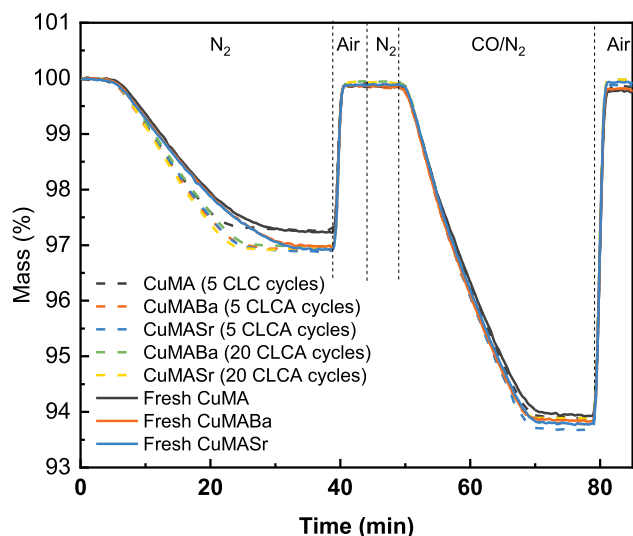
Fig. 9. XRD patterns of OCS composites after 5 and 20 cycles (SR:  $T_{SR} = 900\text{ }^{\circ}\text{C}$ ,  $\text{C}_{\text{H}_2\text{O}} = 60\text{ vol}\%$ ).

was observed located at approx.  $360\text{ }^{\circ}\text{C}$ . For CuMASr, the high-temperature reduction peak (approx.  $400\text{ }^{\circ}\text{C}$ ) also appeared after 5 CLC cycles. The higher reduction temperature could be attributed to the sintering or melting of chlorinated products with low melting points ( $\text{BaCl}_2$ :  $969\text{ }^{\circ}\text{C}$ ,  $\text{SrCl}_2$ :  $874\text{ }^{\circ}\text{C}$ ), which impacted the contact between active phase CuO and CO. Compared with CuMABa, the lower melting point of  $\text{SrCl}_2$  led to more severe deactivation, thus CuMASr had a higher reduction temperature of approx.  $400\text{ }^{\circ}\text{C}$ . After 5 CLCA cycles, the reduction peak was shifted to lower temperature and nearly disappeared after 20 CLCA cycles. Due to the lower regenerability of Sr sorbent, the high-temperature reduction peak was still visible after 5 CLCA cycles, but located at a lower reduction temperature (approx.  $370\text{ }^{\circ}\text{C}$ ). Therefore, for CuMABa and CuMASr, the SR alleviated the deactivation effect of chlorine, and the redox ability remained stable during long-term CLCA cycles.

Generally, the porosities of CuO-based OCs tended to deteriorate after redox cycles due to the thermal sintering [48,51]. The porous properties of the composites before and after cyclic CLCA process are shown in Fig. 12. The BET surface areas of fresh CuMABa and CuMASr were  $8.74$  and  $7.43\text{ m}^2/\text{g}$ , respectively. After 5 cycles, the surface areas were decreased by 24.8% ( $6.57\text{ m}^2/\text{g}$ ) and 19.4% ( $5.99\text{ m}^2/\text{g}$ ), and further decreased to 5.48 and  $5.84\text{ m}^2/\text{g}$  after 20 cycles, respectively. This was accompanied by the decrease in the pore volumes of the

**Table 2**Composition of composite material analyzed by ICP-OES (wt%, converted in metal oxides, SR condition:  $T_{SR} = 900\text{ }^{\circ}\text{C}$ ,  $\text{C}_{\text{H}_2\text{O}} = 60\text{ vol}\%$ ).

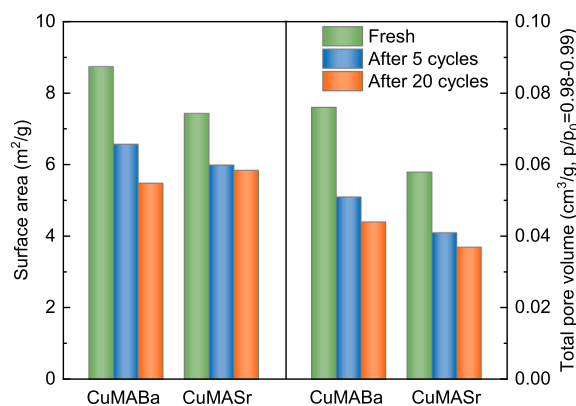
	Fresh			After 5 CLCA cycles		After 20 CLCA cycles	
	CuMA	CuMABa	CuMASr	CuMABa	CuMASr	CuMABa	CuMASr
MgO	18.9	16.4	16.0	16.4	16.0	16.5	16.3
Al <sub>2</sub> O <sub>3</sub>	45.9	39.5	39.5	39.4	39.9	39.3	38.7
CuO	36.0	36.3	36.4	36.4	36.6	35.9	35.6
BaO	–	7.3	–	6.8	–	6.7	–
SrO	–	–	7.9	–	7.9	–	7.8

**Fig. 10.** TGA profiles of composites before and after cyclic CLCA process (SR:  $T_{SR} = 900\text{ }^{\circ}\text{C}$ ,  $\text{C}_{\text{H}_2\text{O}} = 60\text{ vol}\%$ ).

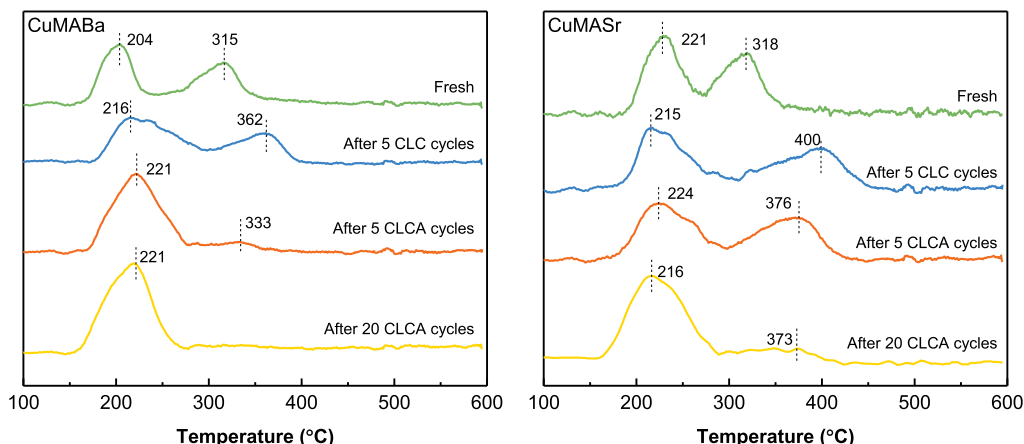
composites as the cycle number. The decrease in porosity could be attributed to the formation of dense surface, which did not influence the combustion activity during 20 cycles. Considering the decrease rate of surface area and pore volume per cycle, the decrease of porosities during 6–20th cycles were much slower than that of 1–5th cycles, suggesting that the porosities of composites were gradually stabilized during cycles.

The crushing strength of composites is shown in Table 3. Generally, an OC is unsuitable for use in an interconnected fluidized bed if its crushing strength is lower than 1.0 N [52,53]. According to the results, the composites exhibited great crushing strength of higher than 4 N. After 5 and 20 cycles, there were no significant changes. Therefore, the synthetic composites in this study had great mechanical strength in the fluidized bed application for chemical looping process.

The XRD, EDS and CO-TPR characterization methods exhibited the outward migration of Cu species during multiple redox cycles, which could be explained by the Kirkendall effect [54,55]. Due to the higher diffusivity of Cu cations than oxygen anions, the oxidation stage drove Cu outward, but the subsequent reduction reaction did not provide a driving force for the Cu cations to diffuse inward [56]. The multiple redox cycles led to the separation of support and Cu within particles and continuous enrichment of Cu on the particle surface [57]. In the current composite particle, the outward diffusion of Cu caused the separation of Cu and MgO and the exsolution of CuO from Cu<sub>2</sub>MgO<sub>3</sub> during redox

**Fig. 12.** Porosities of composite particles before and after CLCA cycles (SR:  $T_{SR} = 900\text{ }^{\circ}\text{C}$ ,  $\text{C}_{\text{H}_2\text{O}} = 60\text{ vol}\%$ ).**Table 3**Crushing strength of fresh and regenerated composites (N, SR:  $T_{SR} = 900\text{ }^{\circ}\text{C}$ ,  $\text{C}_{\text{H}_2\text{O}} = 60\text{ vol}\%$ ).

	Fresh	After 5 CLCA cycles	After 20 CLCA cycles
CuMABa	4.2 ± 1.7	5.2 ± 1.7	5.0 ± 1.6
CuMASr	4.1 ± 1.1	4.2 ± 1.3	4.3 ± 1.4

**Fig. 11.** CO-TPR profiles of composites before and after CLC (without SR) and CLCA (SR:  $T_{SR} = 900\text{ }^{\circ}\text{C}$ ,  $\text{C}_{\text{H}_2\text{O}} = 60\text{ vol}\%$ ) process.

cycle, hence only CuO could be observed in several characterization methods. Although the Kirkendall effect could induce the agglomeration tendency for the particles, it was not enough to cause the deactivation and defluidization during 20 cycles.

#### 4. Conclusion

The performance of HCl removal, syngas combustion, and thermal behavior of Cu-Mg-Al-Ba/Sr composites were investigated. The synthetic composites exhibited great reactivity and stability during multiple CLCA cycles. Nearly full combustion of MSW syngas was achieved with excellent stability during 20 CLCA cycles. The increase of H<sub>2</sub>O content and temperature of SR stage facilitated to regenerate sorbent and lower the HCl emission of FR stage. The SR condition could be optimized at 60 vol% H<sub>2</sub>O content and 900 °C, which would be favorable for auto-thermal operation. The HCl adsorption at FR stage and desorption at SR stage gradually increased at the initial cycles and tended to be stable in the subsequent cycles. CuMABa composite exhibited better HCl adsorption performance than CuMASr during 20 CLCA cycles, owing to its better regenerability.

The porosities, redox abilities and elemental compositions of the composites remained stable during long-term cycles. The migration of Cu/CuO to the particle surface resulted in the slight agglomeration leading to the slight decline of porosity, but avoided the regeneration of Cu<sub>2</sub>MgO<sub>3</sub> and improving the oxygen uncoupling kinetics. The good mechanical strength and the formation of BaAl<sub>2</sub>O<sub>4</sub> and SrAl<sub>2</sub>O<sub>4</sub> stabilized the content of active components (Cu, Ba, Sr), leading to the stable capacities of syngas combustion and HCl adsorption. Therefore, the synthetic Cu-Mg-Al-Ba is a promising composite for CLCA process of MSW syngas.

#### Declaration of Competing Interest

The authors declare that they have no known competing financial interests or personal relationships that could have appeared to influence the work reported in this paper.

#### Acknowledgement

This work is supported by the National Environment Agency, Ministry of Sustainability and Environment, Singapore, under the Waste-to-Energy Competitive Research Programme (WTE CRP 1701 105). The authors also acknowledge the management of Nanyang Environment and Water Research Institute and Economic Development Board, Singapore for the support.

#### Appendix A. Supplementary data

Supplementary data to this article can be found online at <https://doi.org/10.1016/j.cej.2021.132871>.

#### References

- [1] N. Sunny, N. Mac Dowell, N. Shah, What is needed to deliver carbon-neutral heat using hydrogen and CCS? *Energy Environ. Sci.* 13 (11) (2020) 4204–4224.
- [2] M. Ma, X. Ma, W. Cai, W. Cai, Low carbon roadmap of residential building sector in China: Historical mitigation and prospective peak, *Appl. Energy* 273 (2020), 115247.
- [3] H.D. Beyene, A.A. Werkneh, T.G. Ambaye, Current updates on waste to energy (WtE) technologies: a review, *Renew. Energy Focus* 24 (2018) 1–11, <https://doi.org/10.1016/j.ref.2017.11.001>.
- [4] W. Ma, T. Wenga, F.J. Frandsen, B. Yan, G. Chen, The fate of chlorine during MSW incineration: Vaporization, transformation, deposition, corrosion and remedies, *Prog. Energy Combust. Sci.* 76 (2020), 100789, <https://doi.org/10.1016/j.pecs.2019.100789>.
- [5] G. Chen, T. Wenga, W. Ma, F. Lin, Theoretical and experimental study of gas-phase corrosion attack of Fe under simulated municipal solid waste combustion: Influence of KCl, SO<sub>2</sub>, HCl, and H<sub>2</sub>O vapour, *Appl. Energy* 247 (2019) 630–642.
- [6] R.-Z. Zhang, Y.-H. Luo, R.-H. Yin, Experimental study on dioxin formation in an MSW gasification-combustion process: An attempt for the simultaneous control of dioxins and nitrogen oxides, *Waste Manage.* 82 (2018) 292–301, <https://doi.org/10.1016/j.wasman.2018.10.042>.
- [7] D.T. Kearns, Waste-to-Energy with CCS: A pathway to carbon-negative power generation, *Global CCS Ins.* (2019).
- [8] T. Mendiara, F. García-Labiano, A. Abad, P. Gayán, L. de Diego, M. Izquierdo, J. Adánez, Negative CO<sub>2</sub> emissions through the use of biofuels in chemical looping technology: a review, *Appl. Energy* 232 (2018) 657–684.
- [9] A. Lyngfelt, Chemical looping combustion: Status and development challenges, *Energy Fuels* 34 (8) (2020) 9077–9093.
- [10] W.-Z. Bi, R.-D. Zhao, T.-J. Chen, J.-L. Wu, J.-H. Wu, Study on the formation of PCDD/Fs in PVC chemical looping combustion, *J. Fuel Chem. Technol.* 43 (7) (2015) 884–889.
- [11] H. Zhao, J. Wang, Chemical-looping combustion of plastic wastes for in situ inhibition of dioxins, *Combust. Flame* 191 (2018) 9–18, <https://doi.org/10.1016/j.combustflame.2017.12.026>.
- [12] L. Zeng, Z. Cheng, J.A. Fan, L.-S. Fan, J. Gong, Metal oxide redox chemistry for chemical looping processes, *Nat. Rev. Chem.* 2 (11) (2018) 349–364.
- [13] J. Wang, H. Zhao, Chemical looping dechlorination through adsorbent-decorated Fe<sub>2</sub>O<sub>3</sub>/Al<sub>2</sub>O<sub>3</sub> oxygen carriers, *Combust. Flame* 162 (10) (2015) 3503–3515.
- [14] W. Bi, T. Chen, R. Zhao, Z. Wang, J. Wu, J. Wu, Characteristics of a CaSO<sub>4</sub> oxygen carrier for chemical-looping combustion: reaction with polyvinylchloride pyrolysis gases in a two-stage reactor, *RSC Adv.* 5 (44) (2015) 34913–34920.
- [15] S. Enestam, D. Bankiewicz, J. Tuiremo, K. Mäkelä, M. Hupa, Are NaCl and KCl equally corrosive on superheater materials of steam boilers? *Fuel* 104 (2013) 294–306.
- [16] G. Liu, H. Wang, S. Deplazes, A. Veksha, C. Wirz-Töndury, A. Giannis, T.T. Lim, G. Lisak, Ba–Al-decorated iron ore as bifunctional oxygen carrier and HCl sorbent for chemical looping combustion of syngas, *Combust. Flame* 223 (2021) 230–242, <https://doi.org/10.1016/j.combustflame.2020.09.021>.
- [17] H. Wang, G. Liu, Y.Z. Boon, A. Veksha, A. Giannis, T.T. Lim, G. Lisak, Dual-functional witherite in improving chemical looping performance of iron ore and simultaneous adsorption of HCl in syngas at high temperature, *Chem. Eng. J.* 127538 (2020).
- [18] G. Liu, H. Wang, A. Veksha, A. Giannis, T.T. Lim, G. Lisak, Chemical looping combustion-adsorption of HCl-containing syngas using alkaline-earth coated iron ore composites for simultaneous purification and combustion enhancement, *Chem. Eng. J.* 417 (2021), 129226, <https://doi.org/10.1016/j.cej.2021.129226>.
- [19] H. Wang, X. Dou, A. Veksha, W. Liu, A. Giannis, L. Ge, T. Thy Lim, G. Lisak, Barium aluminate improved iron ore for the chemical looping combustion of syngas, *Appl. Energy* 272 (2020), 115236, <https://doi.org/10.1016/j.apenergy.2020.115236>.
- [20] H. Wang, G. Liu, A. Veksha, X. Dou, A. Giannis, T.T. Lim, G. Lisak, Iron ore modified with alkaline earth metals for the chemical looping combustion of municipal solid waste derived syngas, *J. Cleaner Prod.* (2020), 124467, <https://doi.org/10.1016/j.jclepro.2020.124467>.
- [21] E.R. Monazam, R.W. Breault, R. Siriwardane, G. Richards, S. Carpenter, Kinetics of the reduction of hematite (Fe<sub>2</sub>O<sub>3</sub>) by methane (CH<sub>4</sub>) during chemical looping combustion: A global mechanism, *Chem. Eng. J.* 232 (2013) 478–487.
- [22] E.R. Monazam, R.W. Breault, H. Tian, R. Siriwardane, Reaction kinetics of mixed CuO–Fe<sub>2</sub>O<sub>3</sub> with methane as oxygen carriers for chemical looping combustion, *Ind. Eng. Chem. Res.* 54 (48) (2015) 11966–11974.
- [23] U. Arena, F. Di Gregorio, Gasification of a municipal solid waste in a pilot scale bubbling fluidized bed reactor, (2013).
- [24] S. Begum, M. Rasul, D. Cork, D. Akbar, An experimental investigation of solid waste gasification using a large pilot scale waste to energy plant, *Procedia Eng.* 90 (2014) 718–724.
- [25] M. Rydén, D. Jing, M. Källén, H. Leion, A. Lyngfelt, T. Mattisson, CuO-based oxygen-carrier particles for chemical-looping with oxygen uncoupling – experiments in batch reactor and in continuous operation, *Ind. Eng. Chem. Res.* 53 (15) (2014) 6255–6267, <https://doi.org/10.1021/ie4039983>.
- [26] Z. Xu, H. Zhao, Y. Wei, C. Zheng, Self-assembly template combustion synthesis of a core-shell CuO@TiO<sub>2</sub>-Al<sub>2</sub>O<sub>3</sub> hierarchical structure as an oxygen carrier for the chemical-looping processes, *Combust. Flame* 162 (8) (2015) 3030–3045, <https://doi.org/10.1016/j.combustflame.2015.05.006>.
- [27] I. Adánez-Rubio, S.T. Bararpour, A. Abad, P. Gayán, G. Williams, A. Scullard, N. Mahinpey, J. Adánez, Performance evaluation of a Cu-based oxygen carrier impregnated onto zro<sub>2</sub> for chemical-looping combustion (CLC), *Ind. Eng. Chem. Res.* 59 (15) (2020) 7255–7266.
- [28] X. Wang, T. Xu, X. Jin, Z. Hu, S. Liu, B. Xiao, Z. Chen, M. Hu, CuO supported on olivine as an oxygen carrier in chemical looping processes with pine sawdust used as fuel, *Chem. Eng. J.* 330 (2017) 480–490, <https://doi.org/10.1016/j.cej.2017.07.175>.
- [29] X. Zhu, Q. Intiaz, F. Donat, C.R. Müller, F. Li, Chemical looping beyond combustion—a perspective, *Energy Environ. Sci.* 13 (3) (2020) 772–804.
- [30] Y. Lin, H. Wang, Y. Wang, R. Huo, Z. Huang, M. Liu, G. Wei, Z. Zhao, H. Li, Y. Fang, Review of biomass chemical looping gasification in China, *Energy Fuels* 34 (7) (2020) 7847–7862.
- [31] A. Abad, I. Adánez-Rubio, P. Gayán, F. García-Labiano, L.F. de Diego, J. Adánez, Demonstration of chemical-looping with oxygen uncoupling (CLOU) process in a 1.5kWth continuously operating unit using a Cu-based oxygen-carrier, *Intern. J. Greenhouse Gas Control* 6 (2012) 189–200, <https://doi.org/10.1016/j.ijggc.2011.10.016>.
- [32] M. Arjmand, A.-M. Azad, H. Leion, A. Lyngfelt, T. Mattisson, Prospects of Al<sub>2</sub>O<sub>3</sub> and MgAl<sub>2</sub>O<sub>4</sub>-supported CuO oxygen carriers in chemical-looping combustion (CLC) and chemical-looping with oxygen uncoupling (CLOU), *Energy Fuels* 25 (11) (2011) 5493–5502.

- [33] Q. Imtiaz, M. Broda, C.R. Müller, Structure–property relationship of co-precipitated Cu-rich, Al<sub>2</sub>O<sub>3</sub>- or MgAl<sub>2</sub>O<sub>4</sub>-stabilized oxygen carriers for chemical looping with oxygen uncoupling (CLOU), *Appl. Energy* 119 (2014) 557–565, <https://doi.org/10.1016/j.apenergy.2014.01.007>.
- [34] C. Kuang, S. Wang, M. Luo, J. Zhao, Reactivity study and kinetic evaluation of CuO-based oxygen carriers modified by three different ores in Chemical looping with oxygen uncoupling (CLOU) process, *Chin. J. Chem. Eng.* (2021), <https://doi.org/10.1016/j.cjche.2020.12.027>.
- [35] S. Abuelgasim, W. Wang, T. Li, A. Abdalazeez, Z. Xia, The effect of alkali and alkaline earth metals oxides addition on oxygen uncoupling rate of copper-based oxygen carrier, in: *A kinetic and experimental investigations, Separation and Purification Technology*, 2021, p. 119176.
- [36] W.P. Chan, A. Veksha, J. Lei, W.-D. Oh, X. Dou, A. Giannis, G. Lisak, T.-T. Lim, A hot syngas purification system integrated with downdraft gasification of municipal solid waste, *Appl. Energy* 237 (2019) 227–240.
- [37] Q. Imtiaz, A.M. Kierzkowska, C.R. Müller, Coprecipitated, copper-based, alumina-stabilized materials for carbon dioxide capture by chemical looping combustion, *ChemSusChem* 5 (8) (2012) 1610–1618, <https://doi.org/10.1002/cssc.201100694>.
- [38] M. Izquierdo, F. García-Labiano, A. Abad, A. Cabello, P. Gayán, L. de Diego, J. Adánez, On the optimization of physical and chemical stability of a Cu/Al<sub>2</sub>O<sub>3</sub> impregnated oxygen carrier for chemical looping combustion, *Fuel Process. Technol.* 215 (2021), 106740.
- [39] Y. Jin, A.K. Datye, Phase transformations in iron Fischer-Tropsch catalysts during temperature-programmed reduction, *J. Catal.* 196 (1) (2000) 8–17.
- [40] K.-Y. Lee, Y.-J. Huang, Low CO generation on tunable oxygen vacancies of non-precious metallic Cu/ZnO catalysts for partial oxidation of methanol reaction, *Appl. Catal. B* 150–151 (2014) 506–514, <https://doi.org/10.1016/j.apcatb.2013.12.044>.
- [41] D. Li, X. Liu, Q. Zhang, Y. Wang, H. Wan, Cobalt and copper composite oxides as efficient catalysts for preferential oxidation of CO in H<sub>2</sub>-rich stream, *Catal. Lett.* 127 (3) (2009) 377–385.
- [42] Q. Imtiaz, A. Kurlov, J.L.M. Rupp, C.R. Müller, Highly efficient oxygen-storage material with intrinsic coke resistance for chemical looping combustion-based CO<sub>2</sub> capture, *ChemSusChem* 8 (12) (2015) 2055–2065.
- [43] P. Gayán, I. Adánez-Rubio, A. Abad, L.F. de Diego, F. García-Labiano, J. Adánez, Development of Cu-based oxygen carriers for chemical-looping with oxygen uncoupling (CLOU) process, *Fuel* 96 (2012) 226–238, <https://doi.org/10.1016/j.fuel.2012.01.021>.
- [44] C. Zhong, X. Guo, D. Mao, S. Wang, G. Wu, G. Lu, Effects of alkaline-earth oxides on the performance of a CuO–ZrO<sub>2</sub> catalyst for methanol synthesis via CO<sub>2</sub> hydrogenation, *RSC Adv.* 5 (65) (2015) 52958–52965.
- [45] J. Dai, K.J. Whitty, Impact of fuel-derived chlorine on CuO-based oxygen carriers for chemical looping with oxygen uncoupling, *Fuel* 263 (2020), 116780.
- [46] A. Recio, S.C. Liew, D. Lu, R. Rahman, A. Macchi, J.M. Hill, The effects of thermal treatment and steam addition on integrated CuO/CaO chemical looping combustion for CO<sub>2</sub> capture, *Technologies* 4 (2) (2016) 11.
- [47] K. Wang, Q. Yu, Long-lasting investigation of the Cu-based oxygen carrier particles in chemical looping air separation, *Powder Technol.* 343 (2019) 40–48, <https://doi.org/10.1016/j.powtec.2018.11.013>.
- [48] C.R. Forero, P. Gayán, F. García-Labiano, L.F. de Diego, A. Abad, J. Adánez, High temperature behaviour of a CuO/γ-Al<sub>2</sub>O<sub>3</sub> oxygen carrier for chemical-looping combustion, *Int. J. Greenhouse Gas Control* 5 (4) (2011) 659–667, <https://doi.org/10.1016/j.ijggc.2011.03.005>.
- [49] P. Gayán, C.R. Forero, A. Abad, L.F. de Diego, F. García-Labiano, J. Adánez, Effect of support on the behavior of Cu-based oxygen carriers during long-term CLC operation at temperatures above 1073 K, *Energy Fuels* 25 (3) (2011) 1316–1326, <https://doi.org/10.1021/ef101583w>.
- [50] S. Jiang, L. Shen, J. Wu, J. Yan, T. Song, The investigations of hematite-CuO oxygen carrier in chemical looping combustion, *Chem. Eng. J.* 317 (2017) 132–142, <https://doi.org/10.1016/j.cej.2017.01.091>.
- [51] F. Luis, F. Garcá, P. Gayán, J. Celaya, J.M. Palacios, J. Adánez, Operation of a 10 kW<sub>th</sub> chemical-looping combustor during 200 h with a CuO–Al<sub>2</sub>O<sub>3</sub> oxygen carrier, *Fuel* 86 (7–8) (2007) 1036–1045.
- [52] A. Cabello, P. Gayán, F. García-Labiano, L. De Diego, A. Abad, J. Adánez, On the attrition evaluation of oxygen carriers in chemical looping combustion, *Fuel Process. Technol.* 148 (2016) 188–197.
- [53] M. Johansson, T. Mattisson, A. Lyngfelt, Investigation of Fe<sub>2</sub>O<sub>3</sub> with MgAl<sub>2</sub>O<sub>4</sub> for chemical-looping combustion, *Ind. Eng. Chem. Res.* 43 (22) (2004) 6978–6987.
- [54] A. Mishra, F. Li, Chemical looping at the nanoscale—challenges and opportunities, *Curr. Opin. Chem. Eng.* 20 (2018) 143–150.
- [55] A. Smigelskas, Zinc diffusion in alpha brass, *Trans. AIME* 171 (1947) 130–142.
- [56] Y. Qin, Y. Yang, R. Scholz, E. Pippel, X. Lu, M. Knez, Unexpected oxidation behavior of Cu nanoparticles embedded in porous alumina films produced by molecular layer deposition, *Nano Lett.* 11 (6) (2011) 2503–2509.
- [57] Q. Imtiaz, A. Armutlulu, F. Donat, M.A. Naeem, C.R. Müller, Preventing agglomeration of CuO-based oxygen carriers for chemical looping applications, *ACS Sustain. Chem. Eng.* 9 (17) (2021) 5972–5980.